IWSCFF-Paper-2010-2-2

ORBIT EVOLUTION, MAINTENANCE AND DISPOSAL OF SPACECHIP SWARMS

Camilla Colombo[1], Charlotte Lücking[1], Colin R. McInnes[1]
[1]University of Strathclyde, Glasgow, UK, G1 1XJ
camilla.colombo@strath.ac.uk*

ABSTRACT

The combined effect of solar radiation pressure and atmospheric drag is investigated for future mission concepts for swarms of satellites-on-a-chip (SpaceChips). The natural evolution of the swarm is exploited to perform spatially distributed measurements of the upper layers of the atmosphere. The energy gain from asymmetric solar radiation pressure can be used to balance the energy dissipation from atmospheric drag. An algorithm for long-term orbit control is then designed, based on changing the reflectivity coefficient of the SpaceChips. The subsequent modulation of the solar radiation pressure allows stabilisation of the swarm in the orbital element phase space. It is shown that the normally short orbit lifetime for such devices can be extended through the interaction of solar radiation pressure and atmospheric drag and indeed selected and the end-of-life re-entry of the swarm can be ensured, by exploiting atmospheric drag.

KEYWORDS：SpaceChip, solar radiation pressure, equilibrium orbits, swarm, phase space.

1 INTRODUCTION

In recent years, micro-electronics and wireless communication has allowed considerable advances in miniaturisation. Autonomous sensing, computing, and communication systems can be packed into millimetre-sized ‘smart dust’ devices for distributed wireless sensor networks [1], while smaller silicon-based systems down to micron-size have been synthesized [2]. The future application of these technologies to space missions can be envisaged, to address goals that cannot be met with larger systems. By leveraging existing silicon production capabilities, functional devices have been built for space application, which integrate power, attitude determination and control, communication subsystems and payload into a microchip spacecraft, i.e., satellite-on-a-chip (SpaceChip) [3-4].

Low-cost manufacturing offers the benefit of fabrication of vast numbers of SpaceChips. Moreover, miniaturisation overcomes limitations imposed by launch and deployment costs, since such devices could be injected into orbit from a conventional spacecraft or a CubeSat. The deployment of vast numbers of SpaceChips could enable new mission concepts, such as global sensor networks for remote sensing, distributed communications, multi-point, real-time sensing for space science or deployment in the vicinity of a conventional spacecraft for diagnostic or environmental detection purposes. As an early example of a SpaceChip-scale swarm, project West Ford in 1963 placed a ring of 4.8×10^8 copper dipole antennas (1.78 cm long needles, with a diameter of 17.8 μm) into orbit to allow global radio communication [5]. More recently, a mission concept for the distributed measurement of the radiation and temperature on a planetary body (Moon and Mars) has been investigated, through the dispersion of a number of solid state sensor nodes in close vicinity of the planet surface [6].

The realisation of SpaceChip swarm concepts must take into account orbital dynamics at extremely small spacecraft length-scales. Due to the significantly higher area-to-mass ratio with respect to conventional spacecraft, surface forces such as Solar Radiation Pressure (SRP) and atmospheric drag have an important influence on orbit evolution. The secular effect of

these natural perturbations can be exploited as a means of enabling long-lived orbits for SpaceChip swarms where the energy input from asymmetric solar radiation pressure is used to offset the energy dissipation due to atmospheric drag. A condition for Sun-synchronous apse-line precession can be achieved passively without the use of active control [7]. Due to the large area-to-mass ratio of these devices their orbit lifetime due to air drag alone is extremely short. However, the orbit lifetime can be extended by exploiting SRP, but remains anyway limited by the effect of atmospheric drag. Indeed the end-of life behaviour of the swarm can be designed, through passive re-entry. Based on these new insights, a mission concept was proposed for a future SpaceChip swarm mission for the mapping and study of the upper layers of the Earth's atmosphere [8]. A number of small devices are released from a conventional spacecraft and passive orbit evolution under solar radiation pressure and atmospheric drag is exploited to disperse the sensor nodes to perform spatially distributed measurements of the ionosphere and exosphere.

In this paper we extend this mission concept by including active orbit control over the long-term evolution of the swarm. An electro-chromic coating of the SpaceChip device can be employed to alter the reflectivity coefficient of the spacecraft between two set values ($c_{R\,\mathrm{on}} = 1.8$ and $c_{R\,\mathrm{off}} = 1$) [9]. In this way the effect of SRP can be modulated to stabilise the spacecraft on a non-equilibrium orbit. The control relies on a simple algorithm: the spacecraft follow the natural flow lines in the orbital element phase space for the major part of their evolution, and, when the stabilisation region is reached, the reflectivity change is performed once per orbit. The effect of natural perturbations can be exploited to design operational orbits for SpaceChip devices: in the first phase of the mission, solar radiation pressure is exploited to raise the orbit pericentre, whereas in the second phase the dominant effect of drag is used for orbit decay and passive removal of the swarm. The initial conditions for deployment are selected such that a number of distributed measurements can be performed in a defined region of the phase space. The controlled evolution of the swarm is demonstrated against passive orbit evolution and a future mission application is identified which exploits such formation-flying on a large-scale system.

2 ORBIT EVOLUTION

The orbit evolution of the spacecraft is computed through an averaging technique with Gauss' planetary equations to obtain the secular variation of the orbital elements. As a first approach, we consider only solar radiation pressure and atmospheric drag. Although a summary of the analytical model of the orbital dynamics is given in this section, reference [7] provides a more detailed explanation and the validation of the model.

2.1 Solar radiation pressure

We consider a spacecraft on an Earth-centred orbit lying in the ecliptic plane as represented in Figure 1. The satellite is subjected to an acceleration due to solar radiation pressure given by

$$\begin{cases} a_{r,\,\mathrm{SRP}} = a_{\mathrm{SRP}} \cos(\phi + f) \\ a_{\theta,\,\mathrm{SRP}} = -a_{\mathrm{SRP}} \sin(\phi + f) \end{cases} \tag{1}$$

where a_r and a_θ are the components of the acceleration along the radial and transverse direction in the orbital plane, and a_{SRP} is the characteristic acceleration

$$a_{\mathrm{SRP}} = c_R \frac{p_{\mathrm{SR}} A_{\odot}}{m} \tag{2}$$

where $p_{\mathrm{SR}} = 4.56\times10^{-6}\ \mathrm{N/m^2}$ is the solar pressure at 1 AU, c_{R} the reflectivity coefficient, $A_{\odot}$ is the area facing the Sun, and m is the mass of the satellite. The angle $\phi = \omega - \lambda_{\mathrm{Sun}}$ represents the angular displacement between the orbit pericentre ω and the Sun-Earth line direction λ_{Sun}, and f is the true anomaly.

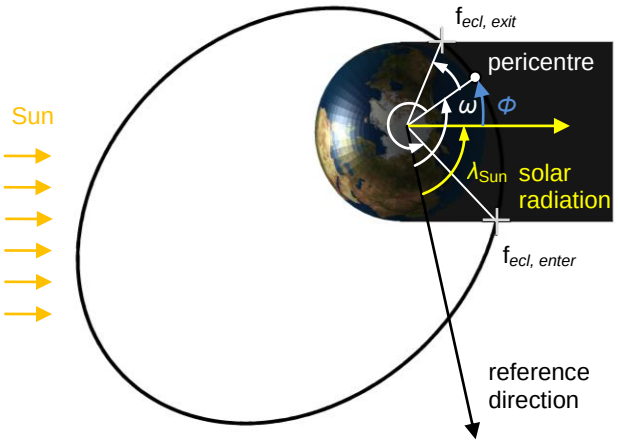

Figure 1: Orbit geometry.

The effect of SRP on the spacecraft orbit can be expressed in terms of the secular variation of the in-plane orbital elements (semi-major axis a, eccentricity e and anomaly of the pericentre ω) on a single orbit revolution, over the orbit arc in which the spacecraft is in sunlight $\left[0,\ f_{\mathrm{ecl,enter}}\right], \left[f_{\mathrm{ecl,\,exit}},\ 2\pi\right]$:

$$\begin{aligned}
\Delta a_{\mathrm{SRP},\,2\pi}\left(a,\,e,\,\phi,\,f_{\mathrm{ecl,\,exit}},\,f_{\mathrm{ecl,\,enter}}\right) &= \left[\mathrm{f}_a\right]_{f_{\mathrm{ecl,\,exit}}}^{f_{\mathrm{ecl,\,enter}}} \\
\Delta e_{\mathrm{SRP},\,2\pi}\left(a,\,e,\,\phi,\,f_{\mathrm{ecl,\,exit}},\,f_{\mathrm{ecl,\,enter}}\right) &= \left[\mathrm{f}_e\right]_{f_{\mathrm{ecl,\,exit}}}^{f_{\mathrm{ecl,\,enter}}} \\
\Delta \omega_{\mathrm{SRP},\,2\pi}\left(a,\,e,\,\phi,\,f_{\mathrm{ecl,\,exit}},\,f_{\mathrm{ecl,\,enter}}\right) &= \left[\mathrm{f}_\omega\right]_{f_{\mathrm{ecl,\,exit}}}^{f_{\mathrm{ecl,\,enter}}}
\end{aligned} \tag{3}$$

with the primitive functions f_a, f_e, f_ω given by:

$$\begin{aligned}
\mathrm{f}_a &= -\frac{2a^3\left(1-e^2\right)}{\mu_{\mathrm{Earth}}} a_{\mathrm{SRP}} \frac{1}{e\left(1+e\cos f\right)}\left(\cos\phi + e\sin\phi\sin f\right) + c_a \\
\mathrm{f}_e &= \frac{a^2\left(1-e^2\right)^2}{\mu_{\mathrm{Earth}}} a_{\mathrm{SRP}} \left(\sin\phi \left(\frac{\sin f\left(\cos f\left(-8e^4+10e^2-2\right)+6e\left(1-e^2\right)\right)}{4\left(1-e^2\right)^2\left(1+e\cos f\right)^2} + \right.\right. \\
&\qquad \left.\left. -\frac{3}{2}\frac{E}{\left(1-e^2\right)^{3/2}} \right) - \frac{\cos\phi}{2e^2\left(1+e\cos f\right)^2}\left(1+2e\cos f+e^2\right) \right) + c_e \\
\mathrm{f}_\omega &= -\frac{a^2\left(1-e^2\right)^2}{\mu_{\mathrm{Earth}} e} a_{\mathrm{SRP}} \left(\cos\phi \left(\frac{3}{2}\frac{E}{\left(1-e^2\right)^{3/2}} - \frac{e\sin f}{\left(1-e^2\right)\left(1+e\cos f\right)} + \right.\right. \\
&\qquad \left.\left. -\frac{1}{2}\frac{\left(e+\cos f\right)\sin f}{\left(1-e^2\right)\left(1+e\cos f\right)^2} \right) + \sin\phi\frac{1+2e\cos f}{2e^2\left(1+e\cos f\right)^2} \right) + c_\omega
\end{aligned} \tag{4}$$

where E is the eccentric anomaly and μ_{Earth} the gravitational parameter of the Earth. Note that Eqs. (4) assume that the disturbing acceleration a_{SRP} is constant when the spacecraft is

in sunlight, i.e., the variation of the solar flux over time is neglected, and the exposed area $A_\odot$ in Eq. (2) is considered constant. The variation of the orbital elements Eqs. (3) is a function of *a*, *e*, ϕ at the orbit pericentre. The arguments of true anomaly at which the satellite enters and exits the Earth's shadow $f_{\text{ecl, exit}}\left(a,e,\omega-\lambda_{\text{Sun}}\right)$ and $f_{\text{ecl, enter}}\left(a,e,\omega-\lambda_{\text{Sun}}\right)$ can be expressed as a closed-form function of the orbital elements [7]. In the case of no eclipse, Eqs. (3) simplify to the formulation used by McInnes et al. [10] and Oyama et al. [11].

2.2 Atmospheric drag

For spacecraft orbits with a low perigee the motion is also influenced by atmospheric drag acceleration as:

$$\mathbf{a}_{\text{Drag}} = -\frac{1}{2}\frac{c_D A_{\text{Drag}}}{m}\rho v_{rel}^2 \hat{\mathbf{v}}_{rel} \tag{5}$$

where c_D is the drag coefficient, A_{Drag} [†] is the effective cross-sectional area of the spacecraft and *m* its mass, v_{rel} is the velocity relative to the atmosphere and $\hat{\mathbf{v}}_{rel}$ the corresponding unit vector. The secular variation of the orbital elements due to atmospheric drag is given through a set of semi-analytical equations. If we neglect atmospheric rotation the variation of $\Delta\omega_{\text{Drag, }2\pi}$ due to drag is zero, while the change of the in-plane orbital elements over a single revolution is given by [12]:

$$\begin{aligned}
\Delta e_{\text{Drag, }2\pi} &= -\frac{A_{\text{drag}}c_D}{m}2\pi a\rho_p \exp\left[-\frac{ae}{H}\right]\left\{I_1+\frac{e}{2}\left(I_0+I_2\right)+\right.\\
&\left.-\frac{e^2}{8}\left(5I_1-I_3\right)-\frac{e^3}{16}\left(5I_0+4I_2-I_4\right)+O\left(e^4\right)\right\}\\
\Delta h_{p\ \text{Drag, }2\pi} &= -\frac{A_{\text{drag}}c_D}{m}2\pi a^2\rho_p \exp\left[-\frac{ae}{H}\right]\left\{\left(I_0-I_1\right)-\frac{e}{2}\left(3I_0-4I_1+I_2\right)+\right.\\
&\left.+\frac{e^2}{8}\left(6I_0-11I_1+6I_2-I_3\right)-\frac{e^3}{16}\left(7I_0-12I_1+8I_2-4I_3+I_4\right)+O\left(e^4\right)\right\}\\
\Delta a_{\text{Drag, }2\pi} &= \frac{\Delta h_{p\ \text{Drag, }2\pi}+a\cdot\Delta e_{\text{Drag, }2\pi}}{1-e}\\
\Delta\omega_{\text{Drag, }2\pi} &= 0
\end{aligned} \tag{6}$$

where h_p is the perigee height, ρ_p is the density at perigee, computed assuming an exponential model of the atmosphere [13], *H* is the scale height, I_k are the modified Bessel functions of the first kind [12].

2.3 Secular rate of change of the orbital elements

The secular and long-period rate of change of the orbital elements can be obtained by dividing Eqs. (3) and Eqs. (6) by the Keplerian orbital period, thus giving:

[†] Note that this is assumed to be equal to the SRP area.

$$\begin{aligned}
\frac{d\bar{a}}{dt} &= \frac{\left(\Delta a_{\text{SRP, }2\pi} + \Delta a_{\text{Drag, }2\pi}\right)}{2\pi}\sqrt{\frac{\mu_{\text{Earth}}}{a^3}} \\
\frac{d\bar{e}}{dt} &= \frac{\left(\Delta e_{\text{SRP, }2\pi} + \Delta e_{\text{Drag, }2\pi}\right)}{2\pi}\sqrt{\frac{\mu_{\text{Earth}}}{a^3}} \\
\frac{d\bar{\phi}}{dt} &= \frac{\Delta\omega_{\text{SRP, }2\pi}}{2\pi}\sqrt{\frac{\mu_{\text{Earth}}}{a^3}} - n_{\text{Earth-Sun}}
\end{aligned} \tag{7}$$

where the superscript dash is used to indicate the secular variation. The line of apsides of the orbit will rotate due to the perturbing solar radiation pressure acceleration; its mean rate of precession is expressed in the third of Eqs. (7) with respect to the Sun-Earth line, introducing the orbital rate of the Earth around the Sun $n_{\text{Earth-Sun}}$.

3 LONG-LIVED ORBITS

In Ref. [7] the conditions for long-lived orbits for SpaceChips with solar radiation pressure and atmospheric drag were defined in the orbital elements phase space, and numerical integration of the secular variation of orbital elements Eqs. (7) is used to characterise the long-term evolution of those orbits. In the following section the method to determine equilibrium and partial equilibrium orbits will be summarised and an overview of long-lived orbits for SpaceChips will be given. A detailed analysis of the orbital element change due to solar radiation pressure and drag and a characterisation of families for long-lived orbits is given in [7]. The conditions for equilibrium orbits under the effect of SRP and atmospheric drag is given by system Eq. (8), where the third equation imposes the Sun-synchronous rotation of the apse-line:

$$\begin{cases}
\Delta a = 0: & \Delta a_{\text{SRP, }2\pi} + \Delta a_{\text{Drag, }2\pi} = 0 \\
\Delta e = 0: & \Delta e_{\text{SRP, }2\pi} + \Delta e_{\text{Drag, }2\pi} = 0 \\
\Delta \phi = 0: & \Delta\omega_{\text{SRP, }2\pi} - n_{\text{Earth-Sun}} \cdot 2\pi\sqrt{a^3/\mu_{\text{Earth}}} = 0
\end{cases} \tag{8}$$

It was shown [7] that system Eq. (8) cannot be satisfied if both solar radiation pressure and atmospheric drag are present. If the effect of drag is negligible, equilibrium orbits can be identified under the effect of solar radiation pressure for $\phi = \pi$. When solar radiation pressure and atmospheric drag both have a non-negligible effect on the spacecraft orbit, even if a complete equilibrium is not possible, it is useful to study *partial equilibrium* solutions, in which the Sun-synchronous condition is satisfied and only one variation, either semi-major axis or eccentricity is zero (see [7]).

The solution of Eqs. (8), which identify the initial conditions for equilibrium or partial equilibrium orbits, can be represented in the phase space $\{e \quad \phi \quad h_p\}$, as depicted in Figure 2a. The reflectivity coefficient of the SpaceChips is taken equal to $c_{R\,\text{on}} = 1.8$ and the other parameters are reported in Table 1. The red surface is the solution of the Sun-synchronous condition $\Delta\phi = 0$, while the purple surface on the domain $\pi \le \phi \le 2\pi$ contains the initial conditions for which the variation of the eccentricity due to SRP and drag balances (i.e., $\Delta e = 0$) and the blue surface on the domain $0 \le \phi \le \pi$ represents the solution of $\Delta a = 0$. For an eccentricity higher than approximately 0.115 and perigee height above 900 km, a set of

solutions for system Eq. (8) exists with the condition $\phi = \pi$ (i.e., the three surfaces intersect). Any initial condition along this line represents an equilibrium orbit whose perigee precesses due to SRP alone, as the effect of drag is negligible.

For lower values of the perigee height (approximately below 800 km) no global equilibrium solutions (system Eq. (8)) can be found but only two out of the three equations of system Eq. (8) can be satisfied. For any initial condition chosen in this region, the orbital elements will not remain constant and the orbit will evolve due to SRP and drag.

In Figure 2b the solution of system Eq. (8) considering a lower reflectivity coefficient $c_{R\,\mathrm{off}} = 1$ is superimposed. Note that all the three surfaces are displaced in the phase space, because the effect of solar radiation pressure is lower with respect to the case with $c_{R\,\mathrm{on}} = 1.8$ while the effect of drag is unchanged (i.e., $c_D = 2.1$ is constant). Finally, Figure 2c highlights the initial conditions for partial and global equilibrium orbits [7] with $c_{R\,\mathrm{off}} = 1$ (red line) and $c_{R\,\mathrm{on}} = 1.8$ (blue line).

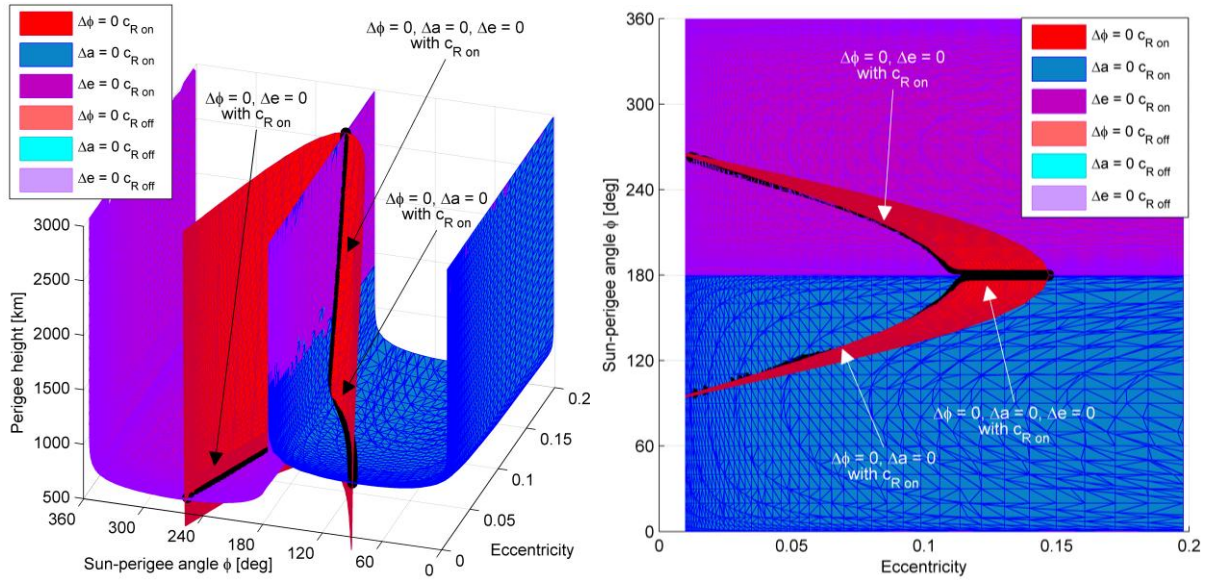

a) 3D view **2D view**

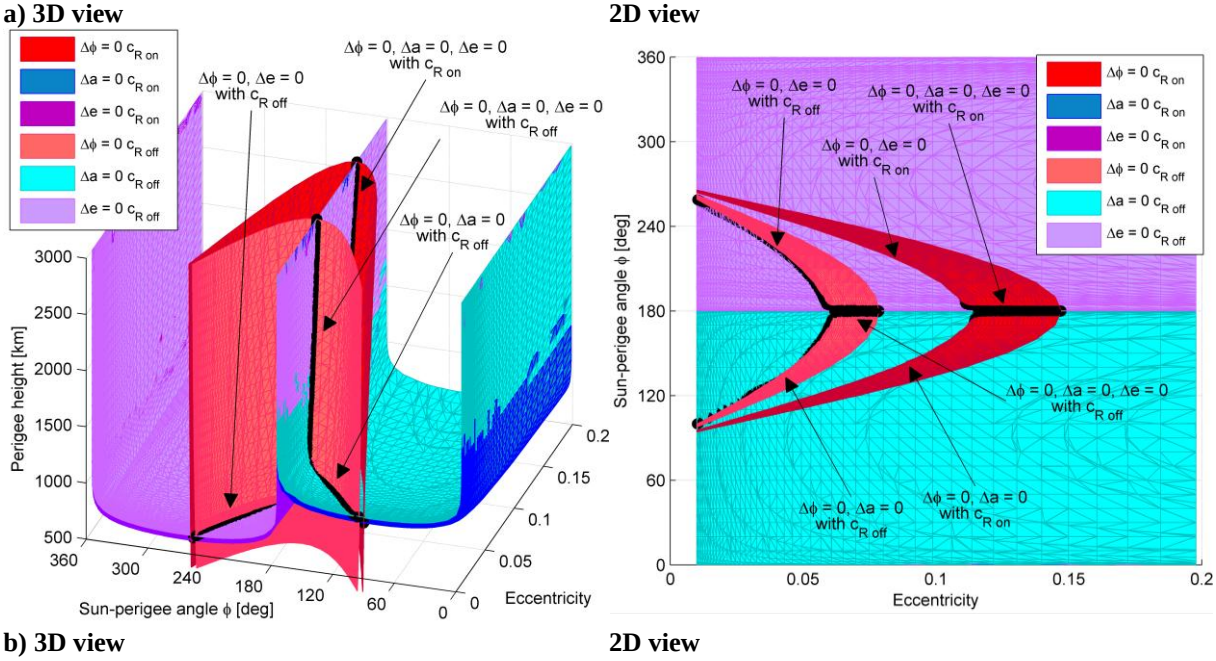

b) 3D view **2D view**

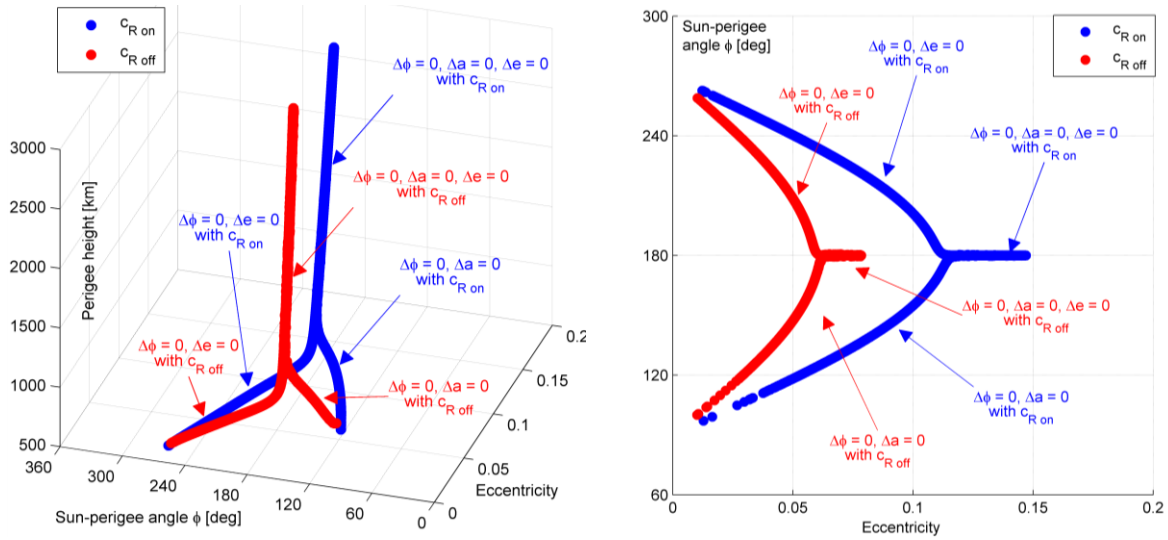

c) 3D view **2D view**

Figure 2: Initial conditions for long-lived orbits. Solutions of Eqs. (8) for a) $c_{R\,\mathrm{on}}$ and b) $c_{R\,\mathrm{off}}$. c) The intersections of the surfaces represent the set of solutions for equilibrium and partial equilibrium orbits.

4 LONG-TERM ORBIT CONTROL THROUGH THE CHANGE OF REFLECTIVITY COEFFICIENT

The long-term evolution of orbits whose initial conditions are represented by the set of points in Figure 2c can be predicted by integrating Eqs. (7). Different families of long-lived orbits were presented [7]. In those regions of the phase space where the effect of atmospheric drag is negligible, equilibrium orbits can be found under the effect of solar radiation pressure only. These solutions correspond to points belonging to the line at $\phi = \pi$ of the surface in Figure 2c, with an initial perigee altitude above some minimum value. If the initial conditions are chosen in a certain region around the equilibrium solution set, the long-term evolution is characterised by *librational motion, progressively decaying* due to the non-conservative effect of atmospheric drag.

Fixing the perigee altitude (or the semi-major axis) it is possible to identify the value of eccentricity (with $\phi = \pi$) for an equilibrium orbit (i.e., an horizontal section of Figure 2c). This is shown in Figure 3 in the case of a SpaceChip with $c_{R\,\mathrm{on}} = 1.8$ (point A) and a SpaceChip with $c_{R\,\mathrm{off}} = 1$ (point B). Excluding for the moment the perturbation due to atmospheric drag, the evolution from a set of initial conditions chosen around the equilibrium points at constant semi-major axis ($a = 8{,}151$ km) is represented. The natural motion is librational around the equilibrium point[‡], with the direction shown by the arrows.

A simple control algorithm can be implemented on a SpaceChip with an electro-chromic coating that switches its reflectivity coefficient between two set values, $c_{R\,\mathrm{on}} = 1.8$ and $c_{R\,\mathrm{off}} = 1$ when a voltage is applied. The use of electro-chromic elements on a solar sail spacecraft was recently successfully tested on the IKAROS mission [14].

$$\begin{cases} c_R = c_{R\,\mathrm{on}} & \text{if } \phi < \pi \\ c_R = c_{R\,\mathrm{off}} & \text{if } \phi \geq \pi \end{cases} \tag{9}$$

In this way the long-term control of the orbit can be achieved and a swarm of SpaceChips, moving along different librational loops, can be stabilised in the phase space at $\phi = \pi$, with an eccentricity between $e_{eq}(c_{R\,\mathrm{off}}) \le e \le e_{eq}(c_{R\,\mathrm{on}})$. Indeed, in correspondence to any point belonging to the segment $\overline{\mathrm{AB}}$ the librational motion with $c_{R\,\mathrm{on}}$ and $c_{R\,\mathrm{off}}$ have an opposite direction (see Figure 3). Once reaching those positions the spacecraft will change its reflectivity value, once per orbit, thus keeping its orbital elements fixed in a position of the phase space which, otherwise, will not be in equilibrium.

The real behaviour, of course, is influenced by atmospheric drag that becomes dominant in the region $e \ge e_{\mathrm{critic}}$ (approximately); e_{critic} is computed as the eccentricity corresponding to a perigee height of 600 km (see Section 5).

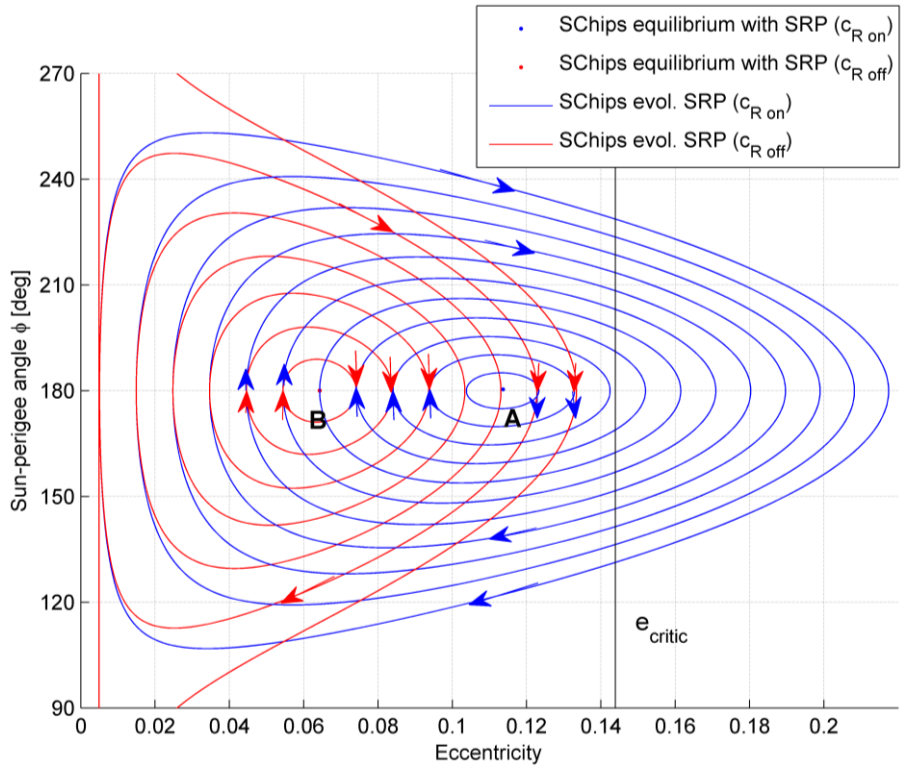

Figure 3: Orbit evolution for initial condition around the equilibrium point with $c_{R\,\mathrm{on}}$ (blue line) and $c_{R\,\mathrm{off}}$ (red line). Only SRP with eclipses is considered for this graph. The effect of drag becomes predominant for eccentricities above e_{critic}.

‡ Note that, due to the presence of eclipses, the semi-major axis along the librational loop is not constant.

5 SPACECHIP SWARM MISSION FOR MAPPING THE EARTH ATMOSPHERE

In Ref. [8] a mission concept was proposed which employs a SpaceChip swarm for mapping the upper layers of the atmosphere (i.e., ionosphere and exosphere). The SpaceChip design by Atchison and Peck [4] is considered (Table 1). The device has a drag coefficient of $c_D = 2.1$ [§] and an electro-chromic coating with variable reflectance is layered on the chip.

Table 1: SpaceChip characteristics.

Parameter	Value
Chip dimensions [mm]	$10 \times 10 \times 0.025$
A/m [m^2/kg]	17.39
c_D	2.1
$c_{R\,\mathrm{on}}$	1.8
$c_{R\,\mathrm{off}}$	1

A larger, conventional spacecraft is injected into an Earth orbit lying in the ecliptic plane, with initial eccentricity of 0.15 and pericentre height of 550 km. The spacecraft motion will be only marginally influenced by solar radiation pressure and atmospheric drag, therefore its orbit will follow for some time a quasi-vertical line in the eccentricity–ϕ phase space (i.e., the orbit apse-line drifts with respect to the Sun-Earth line with a period of one year). As this dispenser spacecraft moves on its orbit, it will release a number of SpaceChips. The period of the year in which the devices are released is chosen such that $127.5 \le \phi \le 180$ deg (i.e., the orbit perigee is in sunlight, the condition $\Delta a > 0$ is satisfied[**]). Because of their high area-to-mass, the SpaceChip devices will not follow the carrier orbit; rather their orbit will evolve under the effect of solar radiation pressure and drag, as described in [7]. Figure 4 represents the phase space coverage of the swarm in two different configurations:

- *Passive evolution* under the effect of drag and solar radiation pressure keeping a constant reflectivity coefficient, $c_{R\,\mathrm{on}} = 1.8$.
- *Long-term controlled evolution* under the effect of drag and solar radiation pressure using the control algorithm Eq. (9).

Reference [8] provides a comparison with the passive evolution under drag only.

The black line corresponds to the orbit of the dispenser spacecraft. In correspondence to the bold black line, a number of SpaceChips can be released from the carrier. The *passive long-term evolution* of the SpaceChips orbits is shown with the thin blue line (Figure 4a). For the first part of the orbit evolution for $\phi < \pi$, $\Delta a > 0$ and $\Delta e < 0$; as a consequence the orbit perigee rises reaching its maximum at $\phi = \pi$. Afterwards, when $\phi > \pi$, $\Delta a < 0$ and $\Delta e > 0$, the perigee height decreases. At a zone below 600 km, the influence of drag becomes predominant and causes the following decay of the orbits[††]. The argument of orbit perigee drifts following the apparent Sun-line rotation, starting behind the Sun for $\phi < \pi$ and moving ahead for $\phi > \pi$. Due to the effect of drag, the spacecraft do not complete the

[§] This value was verified with a Direct Simulation Monte Carlo.

[**] The initial release conditions are selected in order to have a librational evolution [7].

[††] The simulation was stopped at a perigee altitude below 50 km where the last phase of fast decay due to atmospheric drag starts.

librational loop around the equilibrium point (unlike the SRP-only scenario in Figure 3); the motion will follow a *librational and progressively decaying orbit*. Note that, during the whole evolution, the orbit perigee in always in sunlight, allowing communication when the microchip devices pass closer to the Earth surface, or to the carrier spacecraft.

Figure 4a-4c shows the *long-term controlled behaviour* of the swarm. In the first phase of the mission ($\phi < \pi$) the passive evolution is followed ($c_R = c_{R\,\text{on}}$) (see bold light blue line in Figure 4a). Once $\phi \geq \pi$, instead, the reflectivity coefficient if switched to $c_R = c_{R\,\text{off}}$. Hence, the devices will follow different flow lines in the phase space, which librate around the equilibrium line with $c_R = c_{R\,\text{off}}$ (light red Y-shaped line in Figure 4). This phase of the actively-controlled motion is shown in Figure 4b (superimposed on the passive evolution) with thick red lines. As expected form the analysis in Section 4, the spacecraft which, at $\phi = \pi$, have an eccentricity bigger than $e_{eq}\left(c_{R\,\text{off}}\right)$ (and smaller than $e_{eq}\left(c_{R\,\text{on}}\right)$) will stabilise in that position of the phase space. Instead, those spacecraft that, at $\phi = \pi$, have an eccentricity smaller than $e_{eq}\left(c_{R\,\text{off}}\right)$ will not stabilise, and follow the flow lines of $c_{R\,\text{off}}$ (red thick lines) until ϕ reaches again π. If this new point has $e_{eq}\left(c_{R\,\text{off}}\right) \leq e \leq e_{eq}\left(c_{R\,\text{on}}\right)$ the spacecraft will stabilise, otherwise the reflectivity coefficient will switch back to $c_R = c_{R\,\text{on}}$.

Once the spacecraft stabilise in the region $e_{eq}\left(c_{R\,\text{off}}\right) \leq e \leq e_{eq}\left(c_{R\,\text{on}}\right)$, their position in the phase space will not be completely constant due to the effect of drag; rather the stabilised equilibrium points are "dragged" towards lower eccentricities while the radius of the perigee tends to remain constant (see 2D view of Figure 4b). The rate of evolution of this superimposed non-conservative effect depends on the perigee altitude of the stabilised positions.

To avoid the debris hazard of the swarm existing an indefinite time, the duration of the mission is limited to a maximum value $T_{\text{mission max}}$, after which the control algorithm is turned off:

$$\begin{cases} c_R = c_{R\,\text{on}} & \text{if } \phi < \pi \text{ and } t \leq T_{\text{mission max}} \\ c_R = c_{R\,\text{off}} & \text{if } \phi \geq \pi \text{ and } t \leq T_{\text{mission max}} \\ c_R = c_{R\,\text{on}} & \text{if } t > T_{\text{mission max}} \end{cases} \tag{10}$$

In the scenario presented the total mission time was bounded to three years and counted from when the carrier spacecraft starts orbiting with its perigee in Earth shadow. Once $t > T_{\text{mission max}}$ the swarm switches to the flow lines of $c_R = c_{R\,\text{on}}$ and evolves towards a fast decay, due to the effect of atmospheric drag. This last phase of the mission is represented in Figure 4c with thick light blue lines.

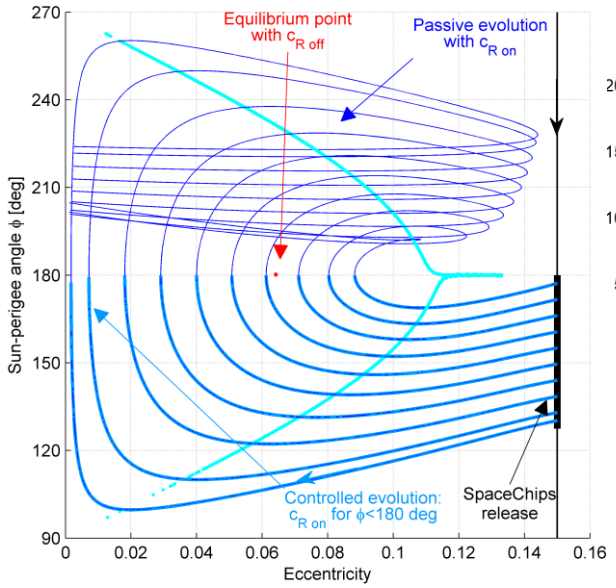

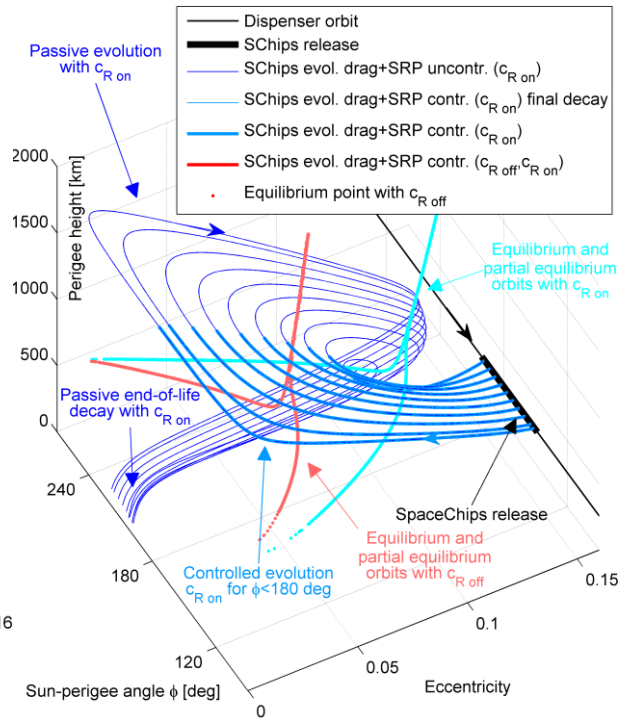

a) 2D view **3D view**

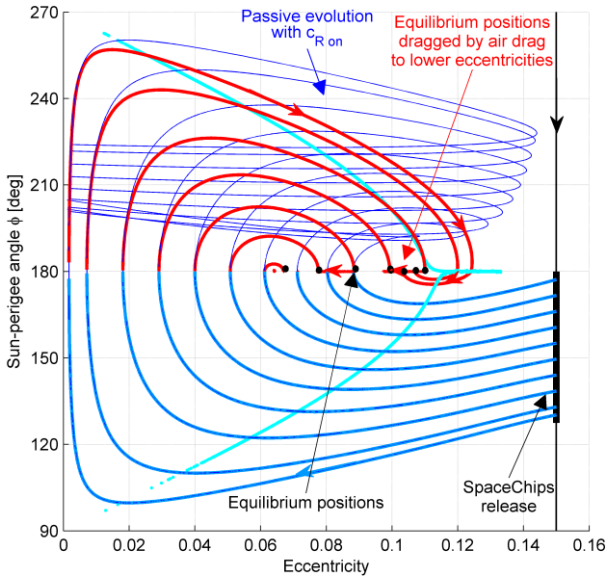

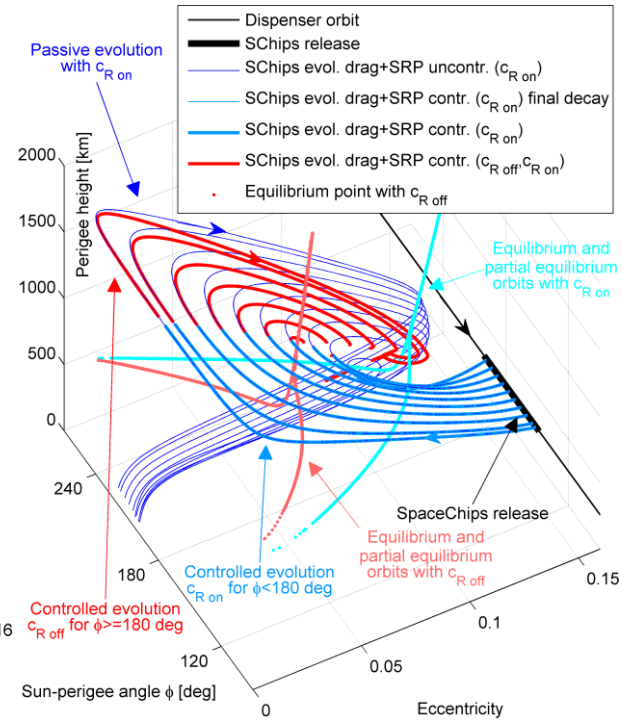

b) 2D view **3D view**

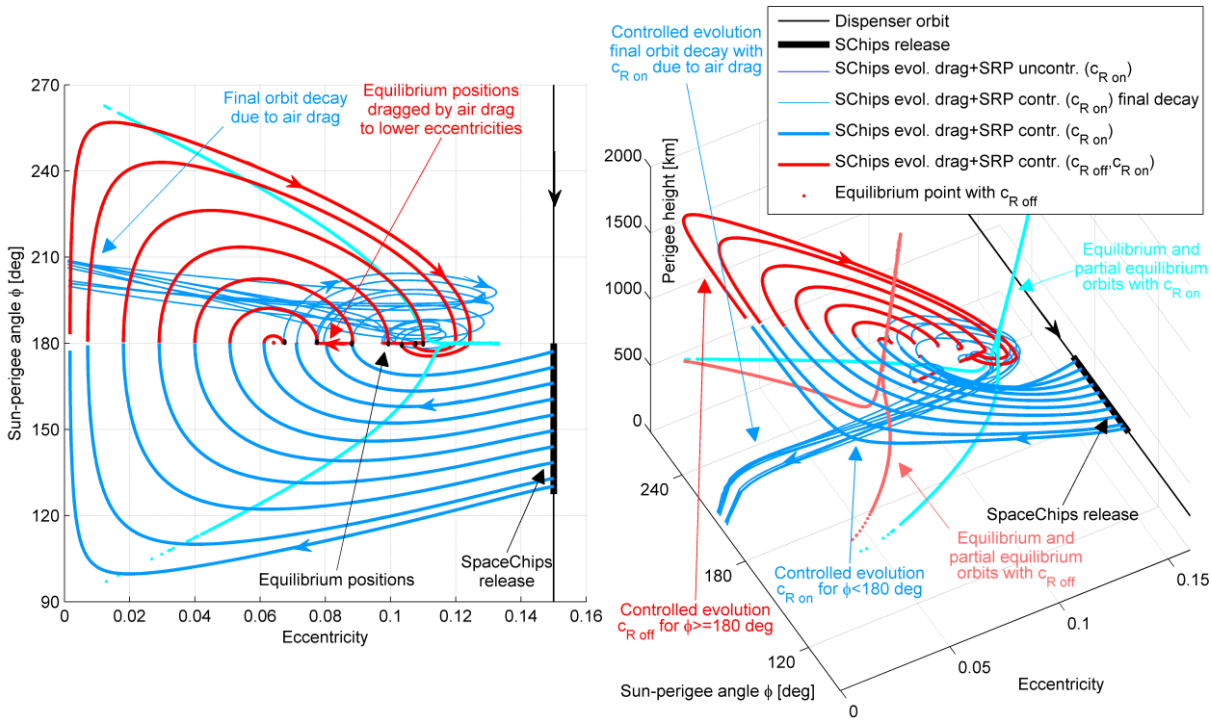

c) 2D view **3D view**

Figure 4: SpaceChip swarm mission. a) *Passive evolution* (thin blue line), and *long-term controlled evolution*. a) Phase 1: initial perigee raising (thick light blue line); b) phase 2: controlled motion (thick red line); c) phase 3: last controlled decay due to air drag (think light blue line).

Figure 5 shows the evolution of the orbital elements with time. The passive exploitation of SRP (blue lines) allows an increase of the perigee height and an extension of the lifetime with respect to the drag-only scenario (green lines) [8]. The control strategy for the reflectivity coefficient allows stabilising the members of the swarm at a constant perigee for a long duration. The selection of the semi-major axis and eccentricity of the release orbit (carrier spacecraft) was driven by the requirement that the swarm stabilises within the exosphere (perigee heights between 640 and 1280 km); however different ranges of altitudes can be explored. The SpaceChips stabilise at $\phi = \pi$, hence the orbit perigee will be in constant sunlight, allowing powering of the spacecraft and communication operations.

At the end-of-mission, the controller is switched off and the swarm naturally decays due to atmospheric drag. This ensures the end-of-life disposal and avoids the creation of long-lived space debris from swarm of devices.

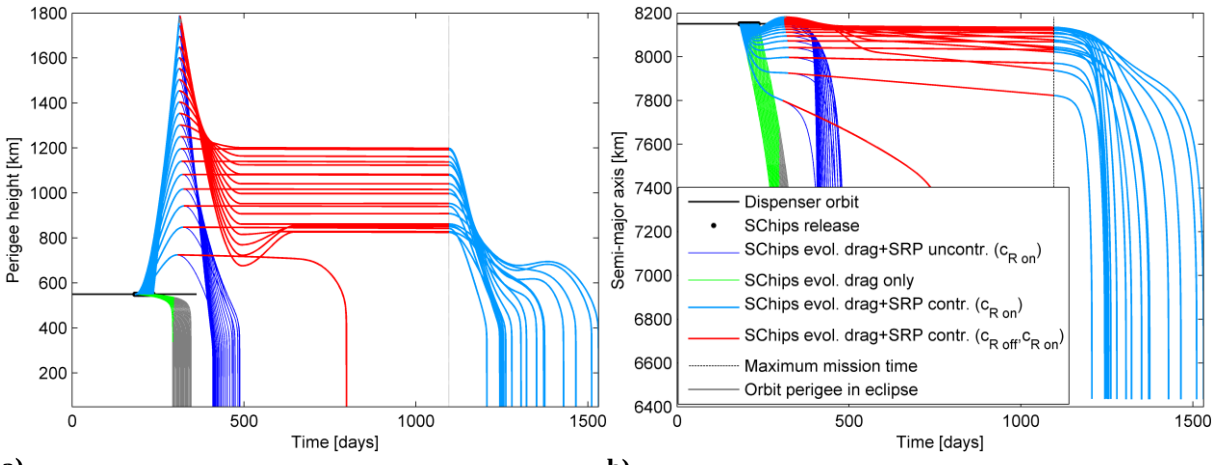

a) **b)**

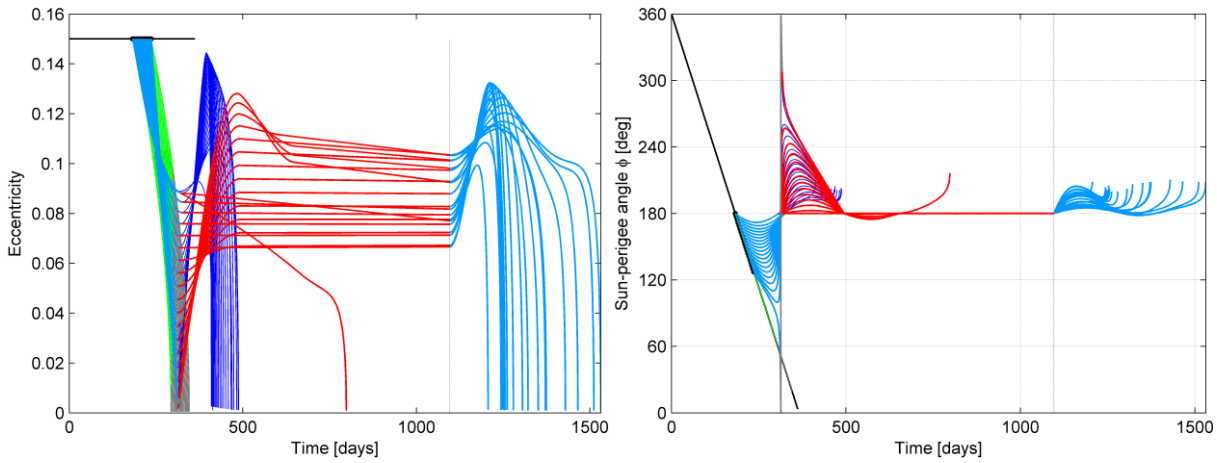

c) d)

Figure 5: Evolution of the swarm orbital parameters in time under the effect of drag-only (green lines), drag and SRP uncontrolled (blue lines), drag and SRP controlled with Eq. (10) (phase 1: light blue lines, phase 2: red lines, phase 3: light blue lines). a) Perigee height, b) semi-major axis, c) eccentricity, and d) Sun-perigee angle ϕ.

Importantly, the effect of SRP causes a significant increase in the orbit lifetime with respect to the drag-only case, as shown in Figure 6, as a function of the angular displacement at release. The lifetime is defined here as the time between the device release from the carrier spacecraft, until the final re-entry below an altitude of 50 km. The green line represents the orbit lifetime of the swarm in the case SRP is not considered ($c_R = 0$), and the blue line corresponds to the passive evolution under drag and SRP with a constant value or reflectivity $c_R = c_{R\,\mathrm{on}}$. If the control strategy in Eq. (9) is implemented, the orbit lifetime of SpaceChips with release conditions of approximately $135 \le \phi \le 175$ deg can be greatly increased (black line). If a maximum mission duration of three years is set, the corresponding swarm lifetime is shown with the red line.

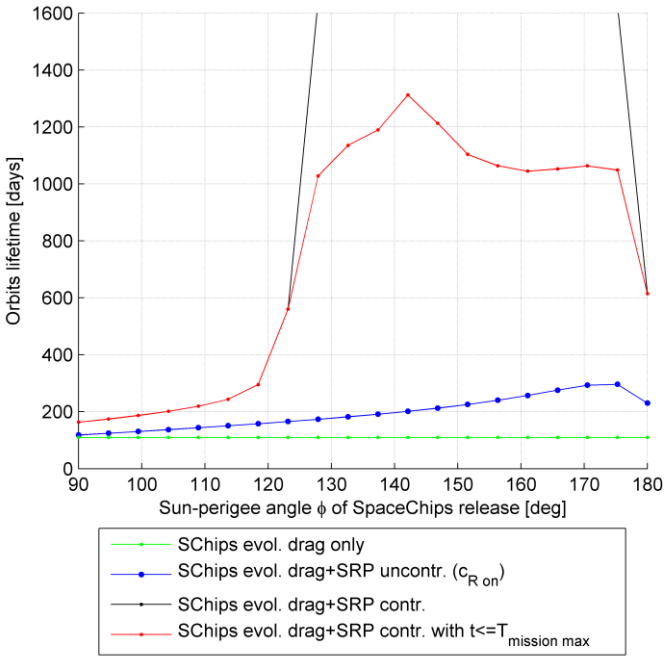

Figure 6: Orbit lifetime as function of the angular position of SpaceChips release under the effect of drag only (green line), drag and SRP uncontrolled with $c_{R\,\mathrm{on}}$ (blue line), drag and SRP controlled (black and red lines).

6 CONCLUSIONS

The modulation of the effect of solar radiation pressure achieved with an electro-chromic coating of the spacecraft allows stabilising a swarm of SpaceChips in a bounded region of the Earth's upper atmosphere. A simple control algorithm which exploits the flow in the orbital element phase space is proposed to extend the mission lifetime. In addition, the effect of

atmospheric drag can be exploited to ensure the end-of-life decay of SpaceChips, thus preventing long-lived orbit debris. It has been shown that the energy gain from asymmetric solar radiation pressure can be used to balance energy dissipation from atmospheric drag to allow the behaviour of swarms of future 'smart dust' devices to be actively designed.

ACKNOWLEDGMENTS

This work was funded by the European Research Council, as part of project VISIONSPACE (227571).

REFERENCES

1. Warneke, B. A. and Pister, K. S. J., "Mems for Distributed Wireless Sensor Networks," *Proceedings of the 9th International Conference on Electronics, Circuits and Systems*, Vol. 1, 2002, pp. 291-294.

2. Sailor, M. J. and Link, J. R., ""Smart Dust": Nanostructured Devices in a Grain of Sand," *Chemical Communications*, No. 11, 2005, pp. 1375-1383.

3. Barnhart, D. J., Vladimirova, T. and Sweeting, M. N., "Very-Small-Satellite Design for Distributed Space Missions," *Journal of Spacecraft and Rockets*, Vol. 44, No. 6, 2007, pp. 1294-1306. doi: 10.2514/1.28678

4. Atchison, J. A. and Peck, M. A., "A Passive, Sun-Pointing, Millimeter-Scale Solar Sail," *Acta Astronautica*, Vol. 67, No. 1-2, 2009, pp. 108-121. doi: 10.1016/j.actaastro.2009.12.008

5. Shapiro, I. I., Jones, H. M. and Perkins, C. W., "Orbital Properties of the West Ford Dipole Belt," *Proceedings of the IEEE*, Vol. 52, No. 5, 1964, pp. 469-518.

6. Graziano, M., Cadenas, R., Medina, A., Puiatti, A., Mura, M., Puccinelli, D., Barrientos, A., Rossi, C., Sanz, D. and Dufour, J.-F., "Distributed Instruments in Preparation to Manned Missions to Mars and Moon," *61st International Astronautical Congress*, Prague, 2010, IAC-10-D3.2.9.

7. Colombo, C. and McInnes, C., "Orbital Dynamics of Earth-Orbiting 'Smart Dust' Spacecraft under the Effects of Solar Radiation Pressure and Aerodynamic Drag," *AIAA/AAS Astrodynamics Specialist Conference 2010*, Toronto, Canada, 2010, AIAA 2010-7656.

8. Colombo, C. and McInnes, R. C., "Orbit Design for Future Spacechip Swarm Missions," *61st International Astronautical Congress*, Prague, 2010, IAC-10-C1.8.2.

9. Lücking, C. M., Colombo, C. and McInnes, C., "Orbit Control of High Area-to-Mass Ratio Spacecraft Using Electrochromic Coating," *61st International Astronautical Congress*, Prague, 2010, IAC-10-C1.2.7.

10. McInnes, C. R., Macdonald, M., Angelopolous, V. and Alexander, D., "Geosail: Exploring the Geomagnetic Tail Using a Small Solar Sail," *Journal of Spacecraft and Rockets*, Vol. 38, No. 4, 2001, pp. 622-629.

11. Oyama, T., Yamakawa, H. and Omura, Y., "Orbital Dynamics of Solar Sails for Geomagnetic Tail Exploration," *Journal of Guidance, Control and Dynamics*, Vol. 45, No. 2, 2008, pp. 316-323. doi: 10.2514/1.31274

12. Blitzer, L., "Handbook of Orbital Perturbations," University of Arizona, 1970.

13. Vallado, D. A., *Fundamentals of Astrodynamics and Applications*, Third Edition, Space Technology Library, New York, 2007.

14. Kawaguchi, J. i., Mimasu, Y., Mori, O., Funase, R., Yamamoto, T. and Tsuda, Y., "Ikaros - Ready for Lift-Off as the World's First Solar Sail Demonstration in Interplanetary Space," *Proceedings of the 60th International Astronautical Congress, IAC 2009*, Daejeon, Korea, 2009, IAC-09-D1.1.3.